Current status of numerical flow prediction for separated nozzle flows

*R. Stark * and G. Hagemann***

*DLR, German Aerospace Center, Lampoldshausen, D-74239, Germany

**Astrium ST, Munich, D-81663, Germany

Abstract

The European 'Flow Separation Control Device' group (FSCD) organized in collaboration with the French 'Aérodynamiques des tuyères et Arrière-Corps' group (ATAC) a CFD workshop with test cases on different nozzle flow topics. One of these test cases (1A) was managed by the German Aerospace Center (DLR) and Astrium ST. The objective was to compute the flow inside a strongly over-expanded truncated ideal contour nozzle with respect to the prediction of location and shape of the flow separation, the oblique shock and the Mach disc. Experimental data were provided by DLR.
An introduction to the test facility and the experimental setup is given. The numerical results are evaluated and compared to test data. A concluding synthesis illustrates the current status of nozzle flow computation.

1. Introduction

Europe's heavy launcher Ariane 5 features a parallel stage design in opposite to a classical tandem configuration like Ariane 4. The main stage engine Vulcain 2 therefore has to fulfil a wider range of operation conditions during ascent. Its nozzle is designed to be full flowing under sea-level conditions to avoid flow separation resulting in side loads. This restriction limits the available expansion area ratio yielding in performance losses during most of the ascent trajectory. Controlling separation and side loads promises a distinct performance gain.

To study both flow separation in classical bell nozzles and altitude adapting rocket nozzles, such as plug nozzles, dual-bell nozzles or nozzles with an extendible exit cone, the 'European Flow Separation Control Device' group (FSCD) was initiated[5]. Within the group the question arose if a bowed Mach disc is present in truncated ideal contour nozzles with a downstream trapped vortex like computed e.g. in ref. 7 and 12. For this reason DLR Lampoldshausen carried out cold flow tests[14] to study the Mach disc in TIC nozzles. One of the obtained data sets was chosen to be computed as FSCD/ATAC workshop test case 1A.

2. Experimental setup

The provided test data were obtained at DLR's cold flow test facility P6.2 in Lampoldshausen, Germany. This test facility features a vertical test position in a high altitude chamber as well as a free-standing horizontal test rig[6]. As fluid dry gaseous nitrogen is used, stored in high pressure tanks outside the facility. The nitrogen flow passes a cylindrical settling chamber (consisting of a honeycomb/screens combination) and a cross-section constriction before it accelerates in a convergent-divergent nozzle to supersonic velocity (fig. 1). Total pressure and total temperature, measured between settling chamber and constriction, were $2.5*10^6 \text{N/m}^2$ and 283K, respectively.
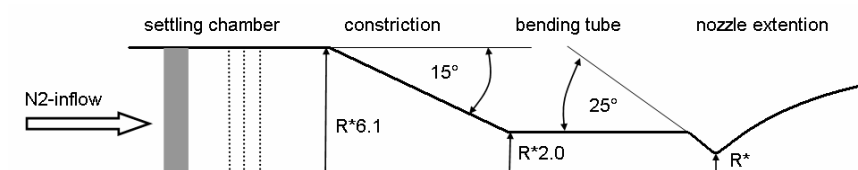

Figure 1: Sketch of horizontal test section.

2.2 Test specimen, instrumentation and data acquisition

The test specimen was a truncated ideal contour (TIC) subscale nozzle made of acrylic glass, with a throat diameter of 20mm, an overall divergent length of 90mm, a wall thickness of 11.5mm, and a design Mach number of 5.15 (described in detail in ref. 4). Its contour was measured in 3 axial planes and the deviation compared to the design contour was less than 5µm. The tests took place on the horizontal test rig where the specimen is positioned 1.2m above the floor.

The specimen was equipped with pressure transducer ports, arranged in stream wise direction with a spacing of 2.5mm each, starting in the nozzle's throat. Using teflon tubes, the ports were connected to XT-154-190M Kulite pressure sensors. The tubing limited the effective frequency response to 330Hz. Therefore the AS2 amplifiers (DLR proprietary) were equipped with a low-pass filter of 160Hz. The sensors were calibrated statically before mounting and their analogue signals were sampled with a rate of 1kHz. The model with its transducer ports is shown in fig. 2.
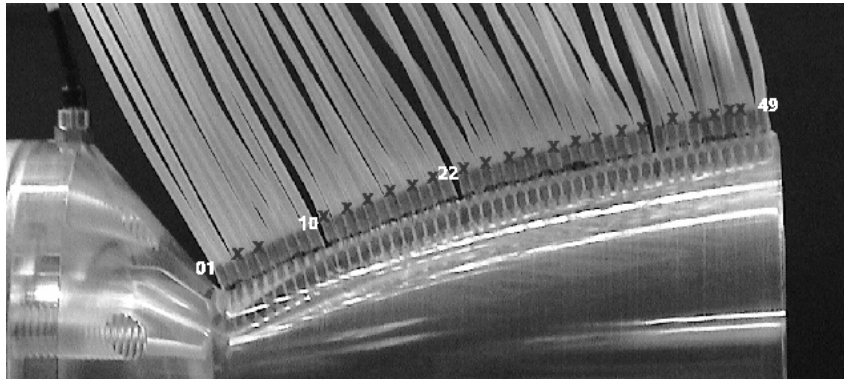

Figure 2: Acrylic glass TIC nozzle with transducer ports[14].

The exhaust jet was investigated with a color schlieren setup based on the dissection technique developed by Cords[3] and improved by Ciezki[2]. Images were taken with a Hasselbad EL 500 camera, digitalized and superimposed with a 3D nozzle contour grid. Calibrated with a well known acrylic glass template before, the shock structure was measured (fig. 3a/b).
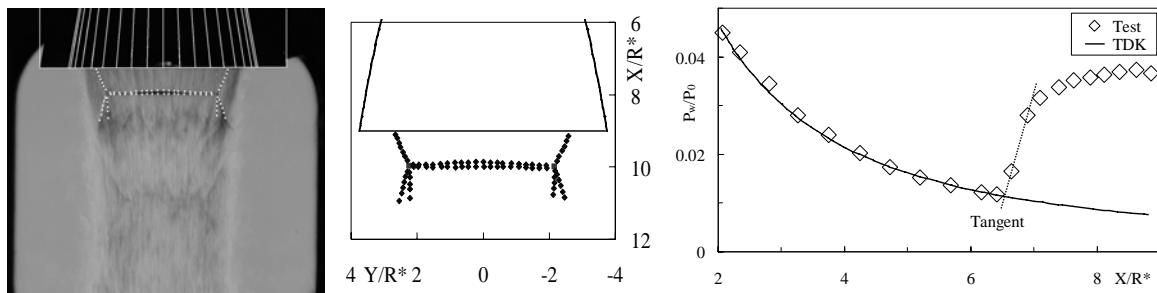

Figure 3: Test case data, a) schlieren image, b) evaluated shock positions, c) nondimensional wall pressure.

2.3 Test data

For p_0/p_a=25.25 the location of the flow separation was obtained by a comparison of the non-dimensional wall pressure data with a non-dimensional vacuum wall pressure profile given by a numerical methods of characteristics (MOC) analysis (fig. 3c). The intersection of a tangent along the steepest wall pressure gradient with the vacuum wall pressure profile marks the axial separation location normalised by the throat radius: X/R^*=6.6.

3. CFD results by comparison, flow separation

The CFD computations differ regarding both the grid, with its structure, initial solution and refinement, and the applied turbulence model. In many cases these computations were conducted using shear stress transport (SST) turbulence models. In case of flow separation, these models under-predict the separation location in a typical range

of -10%, related to the axial position starting in the nozzle's throat. A better agreement with the experimental data is found using standard kω (Wilcox, Sarkar) as well as Spalart-Allmaras models.

Also modifications of the standard SST model were studied, but these modifications don't improve the precision of the separation prediction. Except for a modification suggested by Östlund[10], whose model is validated with VAC cold flow data.

In general the computed locations differ from the experimental one between -34% and +4% with a clear trend to under-predict the flow separation. A comparison of computed and experimental wall pressures p_w, normalized by ambient pressure p_a, versus the axial location X, normalized by the throat radius R*, is given in fig. 4. Included are both a full flowing wall pressure profile obtained by a MOC code and the separation criteria[15] $p_{sep}/p_a=1/Ma_{sep}$, where p_{sep} is the lowest wall pressure upstream the separation zone and Ma_{sep} the related wall Mach number. A detailed comparison is listed in tab. 1.
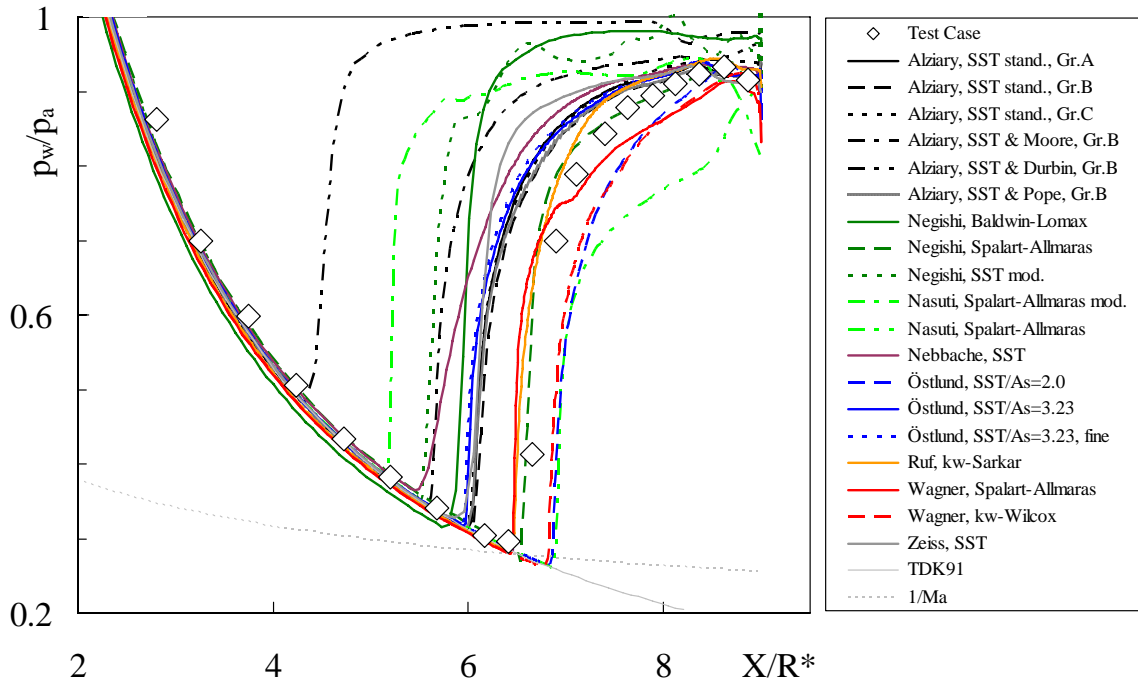

Figure 4: Computed and experimental wall pressures.

As the turbulence model seems to influences only the quantity of the under-prediction, a common reason must be given driving this under-prediction. A hint might be found in fig. 5a where the maximum wall pressure in the separated back flow region p_{bmax} versus the separation location X_{sep}, normalized by the nozzle's divergent length L, is shown. Included are averaged maximum back pressures of the whole test series that show a linear trend. Most of the computations yield a back pressure to high resulting in a premature flow separation. Strongly under-predicting computations show comparable high wall pressures in the back flow. Typically the over-prediction of p_{bmax} is within the range of 1 to 4% (fig. 5b).
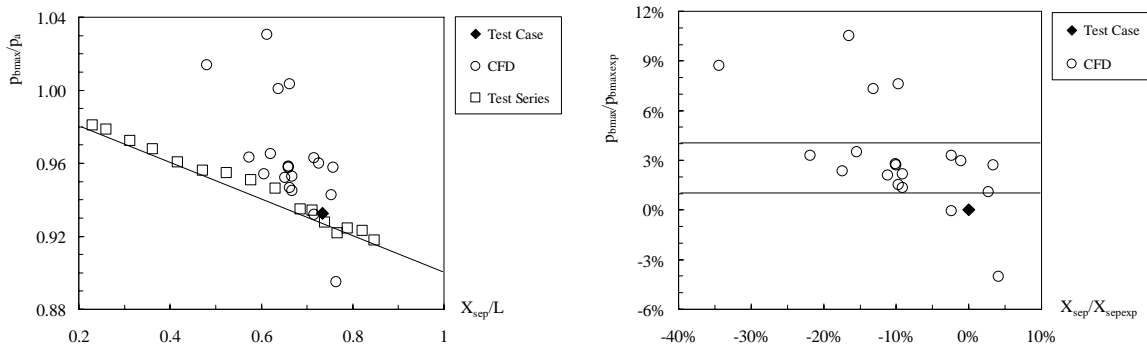

Figure 5: Maximum predicted back flow pressure versus separation location, a) absolute, b) percental.

3.2 Mach disc

The centreline pressure distributions, where the steep gradients mark the related shocks, are given in fig. 6 and tab. 2. Included in fig. 6 is the position of the experimental Mach disc, derived from a schlieren picture. The computed locations differ from the experimental one down to -18%. No over-prediction can be found. Via oblique shock and separation position, the applied turbulence models affect the Mach disc location. Therefore modifying the turbulence model has a comparable negative impact on the precision of the Mach disc prediction. The SST turbulence models under-predict the Mach disc location in a range of -8 to -7%. Östlund's modified SST model predicts once again better. Standard kω and Spalart-Allmaras models reverse their trend of prediction accuracy.
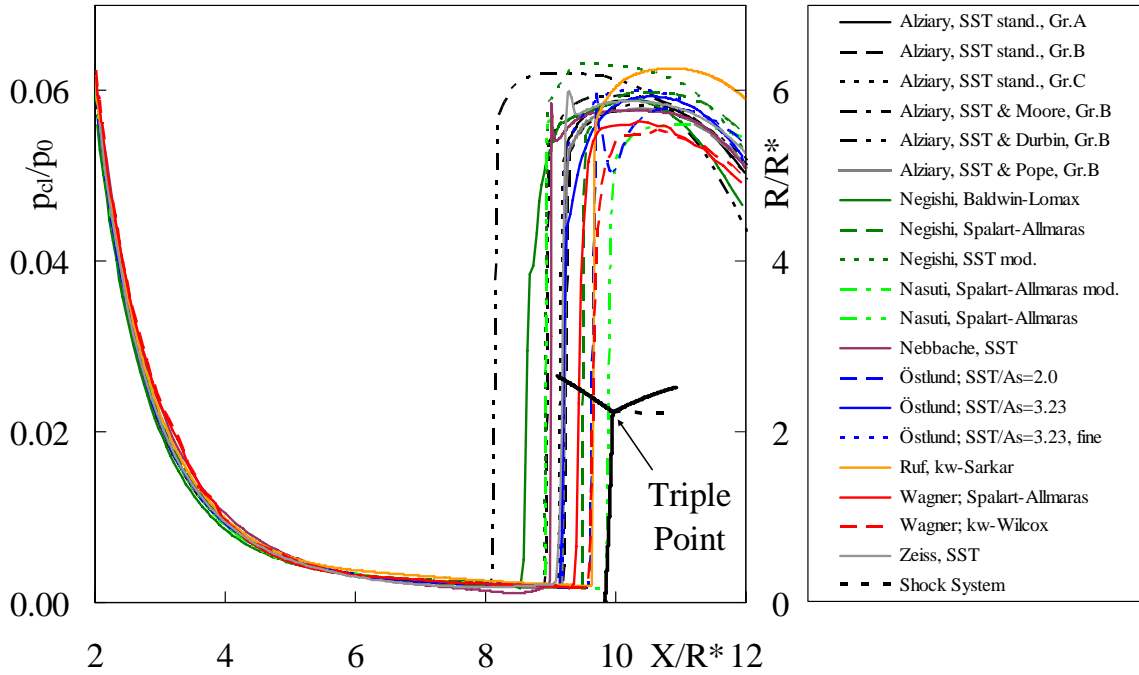

Figure 6: Axial pressures.

Figure 7a gives the absolute positions of the computed triple points, where the oblique shock and the Mach disc merge and a reflected shock is originated, compared to the experimental test data (black diamond). Uncared three exceptions (square, triangles) the computed triple points form out a line. If the displacements of the computed triple points $|Shift_{tr}|$ are compared to the related axial shifts of the separation prediction $X_{sep}-X_{sepexp}$, a linear correlation can be found (fig. 7b). Assuming, the separation location and the triple point position are the two end points defining the oblique separation shock and applying the intercept theorem, the linear correlation found concludes that most of the computations feature an equal shock angle and are in parallel displaced. As this trend doesn't hit the correct separation location, this common shock angle is predicted as to high.
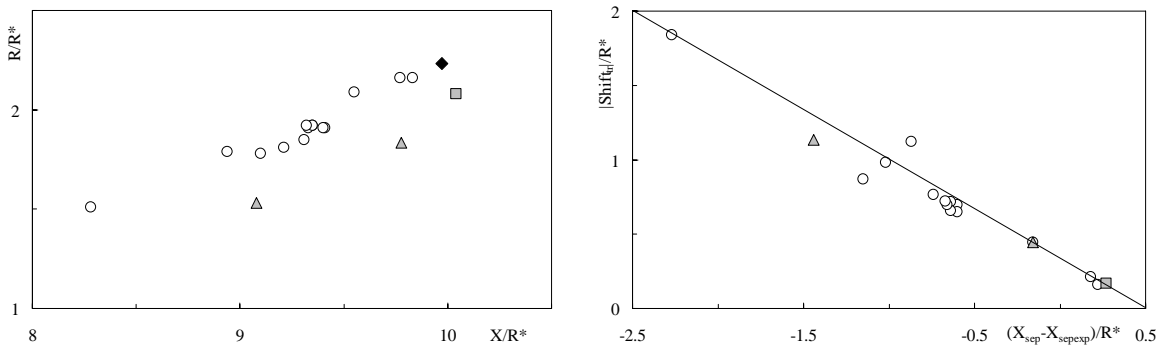

Figure 7: Computed triple point positions, a) absolute compared to test data (black diamond), b) displacement.

3.3 Trapped Vortex

Most of the CFD computations yield no vortex trapped downstream a bended Mach disc. Studies on grid refinement, performed by Wagner[16] (fig. 9)) and Zeiss[18] (fig. 10) point out that the curvature of the Mach disc decreases and the trapped vortex disappears if the cell number is locally increased. Fig. 8a gives the Mach disc radius R_{tr} versus the 'height' of the bended Mach disc, where X_{sh} is the axial position of the Mach disc centre and X_{tr} the axial position of the triple point. Included are the before mentioned grid studies. Computations yielding a vortex are marked with an X. Clear to see the coherence between Mach disc curvature and appearance of the vortex. Fig. 8b gives the radii of the computed vortices as a function of the Mach disc curvature. Vortices are expectedly smaller if the computed Mach disc is less bended.
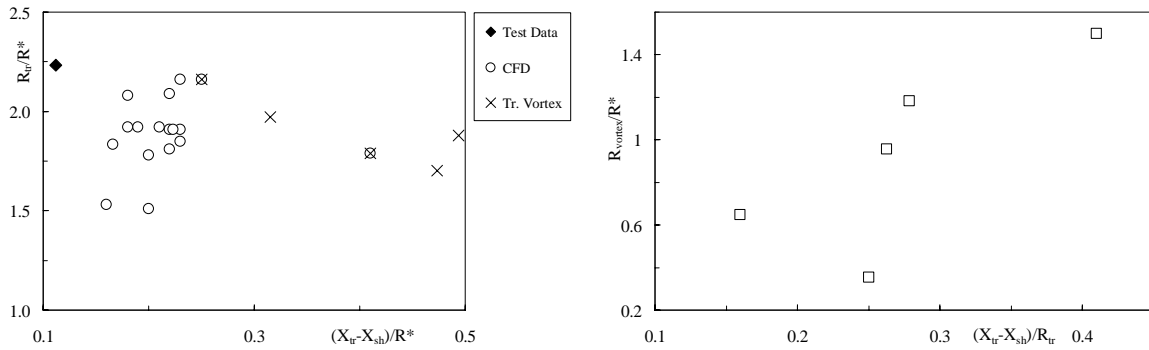
Figure 8: Bended Mach disc, a) disc radius versus height, b) trapped vortex radius versus disc curvature.
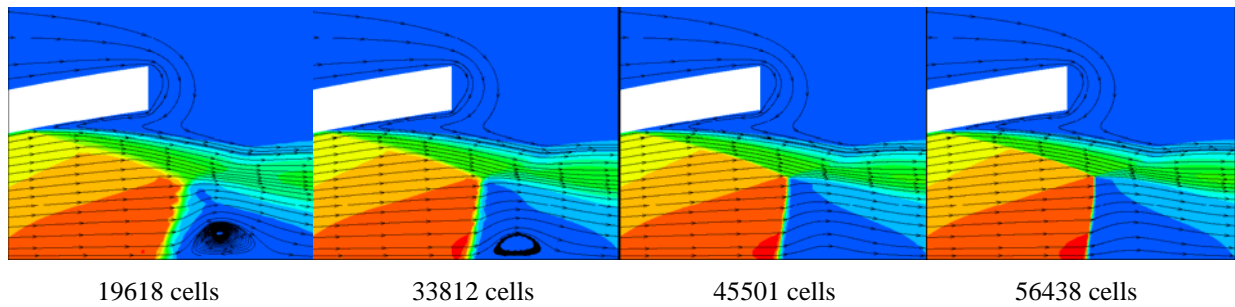

| 19618 cells | 33812 cells | 45501 cells | 56438 cells |

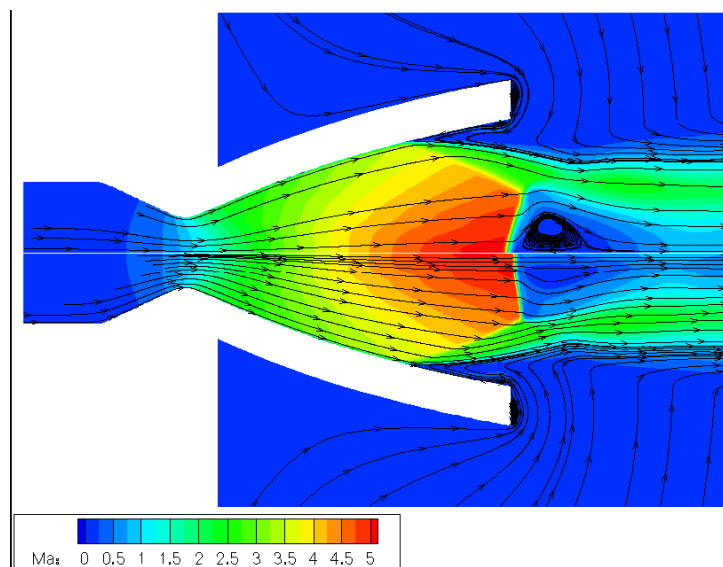Figure 9: Grid study on trapped vortex / Wagner[16], TAU, Spalart-Allmaras.

Figure 10: Grid study on trapped vortex / Zeiss[18], CFX, SST. Upper: 74970 cells, lower: 121400 cells.

4. Conclusion

The evaluation showed that up-to-date CFD simulations (at least for cold flow nozzles) tend to under-predict the separation location. A small advantage arose for kω and Spalart-Allmaras turbulence models and they seem to be a better approach to calculate nozzle flows. Modifications of the standard models weren't successful, except the interesting SST approach of Östlund[10].

Compared to experimental data both the wall pressure in the separated backflow region and the oblique separation shock angle are over-predicted. The over-predicted shock angle results in an increased flow deflection, followed by a stronger jet construction and an increased exit area fraction being available for the back flow of the ambient media. The shock angle is the driver for the quality of the calculated back flow wall pressure distribution. The turbulence model affects not only the boundary layer calculation but also the entrainment capability of the jet's shear layer. It is the driver for the quantity of the calculated back flow. Together, both effects result in the under-predicted separation location.

A strong bowed Mach disc with a trapped vortex is concluded to be artificial and a function of the grid density and structure. Applying a grid refinement decreases the curvature of the Mach disc and shrinks the downstream trapped vortex until its breakup.

5. Acknowledgments

References

[1] Alziary Th. and Deniau H. Contribution to test case 1a, *Proceedings of The FSCD-ATAC Workshop, Noordwijk, 15-16th November, The Netherlands*, 2006

[2] Ciezki, H. Entwicklung eines Farbschlierenverfahrens unter besonderer Berücksichtigung des Einsatzes an einem Stosswellenrohr. *Diploma Thesis, Technical University Aachen, Germany*, 1985.

[3] Cords, P. A High Resolution, High Sensitivity Colour Schlieren Method. *S.P.J.E. Journal, Vol. 6*, 1968.

[4] Frey, M. Behandlung von Strömungsproblemen in Raketendüsen bei Überexpansion. *Ph. D. Thesis, Universität Stuttgart*, 2001.

[5] Frey M. et.al. Joint european effort towards advanced rocket thrust chamber technology. *6th International Conference on Launcher Technologies*, November 2005

[6] Kronmüller H., Schäfer K., Zimmermann H. and Stark R. Cold gas subscale test facility P6.2 at DLR Lampoldshausen. *6th Symposium on Propulsion for Space Transportation of the XXIth century, Versailles*, 2002.

[7] Nasuti F., Onofri M. and Pietropoli E. Prediction of shock generated vortices in rocket nozzles. *AIAA Paper 2005-317*, 2005.

[8] Nebbache A. Test case 1a, *Proceedings of The FSCD-ATAC Workshop, Noordwijk, 15-16th November, The Netherlands*, 2006

[9] Negishi H., Shimizu T., Yamanishi N. and Tsuboi N. Numerical Simulation of the test case 1a, *Proceedings of The FSCD-ATAC Workshop, Noordwijk, 15-16th November, The Netherlands*, 2006

[10] Östlund J. and Krey F. The FSCD-ATAC workshop; CFD simulation of test case 1a, *Proceedings of The FSCD-ATAC Workshop, Noordwijk, 15-16th November, The Netherlands*, 2006

[11] Onofri M., Nasuti F., Martelli E. and Fittipaldi A. The FSCD-ATAC workshop; contribution to test case 1a, *Proceedings of The FSCD-ATAC Workshop, Noordwijk, 15-16th November, The Netherlands*, 2006

[12] Pilinski C. and Nebbache A. Flow separation in a truncated ideal contour nozzle. *Journal of Turbulence, Vol.20, No.3*, 2004

[13] Ruf J. H. NASA/MSFC's Calculation for Test Case 1a of ATAC-FSCD Workshop on After-body and Nozzle Flows, *Proceedings of The FSCD-ATAC Workshop, Noordwijk, 15-16th November, The Netherlands*, 2006

[14] Stark R. and Wagner B. Experimental flow investigation of a truncated ideal contour nozzle. *AIAA Paper 2006-5208*, 2006

[15] Stark R. and Wagner B. Mach disk shape in truncated ideal contour nozzles. *26th International Symposium on Shock Waves, Göttingen, 15-20thJuly, Germany*, 2007

[16] Wagner B., Karl S. and Hannemann K. Test Case 1a: Short Nozzle Under Separated Flow Condition; Numerical Investigation with the DLR Tau-Code, *Proceedings of The FSCD-ATAC Workshop, Noordwijk, 15-16th November, The Netherlands*, 2006

[17] Wong H. Flow structure with DLR TIC Nozzle (testcase 1a), *Proceedings of The FSCD-ATAC Workshop, Noordwijk, 15-16th November, The Netherlands*, 2006

[18] Zeiss W. and Behr R. ATAC-FSCD workshop "after-body and nozzle flows" test case 1a, *Proceedings of The FSCD-ATAC Workshop, Noordwijk, 15-16th November, The Netherlands*, 2006

Table 1: Comparison of separation location

	Separation	Offset	SST	SST	Spalart	Baldwin	kω	kω
	X_{sep}/R^*	X_{sepCFD}/X_{sepexp}	standard	modified	**Allmaras**	**Lomax**	Wilcox	Sarkar
Experiment	6.6							
Alziary, SST stand., Gr.A	6	-9.1%	-9.1%					
Alziary, SST stand., Gr.B	6	-9.1%	-9.1%					
Alziary, SST stand., Gr.C	5.960	-9.7%	-9.7%					
Alziary, SST & Moore, Gr.B	5.58	-15.5%		-15.5%				
Alziary, SST & Durbin, Gr.B	4.33	-34.4%		-34.4%				
Alziary, SST & Pope, Gr.B	5.96	-9.7%		-9.7%				
Negishi, Baldwin-Lomax	5.73	-13.2%				-13.2%		
Negishi, Spalart-Allmaras	6.53	-1.1%			-1.1%			
Negishi, SST mod.	5.51	-16.5%		-16.5%				
Nasuti, Spalart-Allmaras mod.	5.16	-21.8%			-21.8%			
Nasuti, Spalart-Allmaras	6.87	4.1%			4.1%			
Nebbache, SST	5.45	-17.4%	-17.4%					
Östlund, SST/As=2.0	6.82	3.3%		3.3%				
Östlund, SST/As=3.23	5.94	-10.0%	-10.0%					
Östlund, SST/As=3.23, fine	5.93	-10.2%	-10.2%					
Ruf, kω-Sarkar	6.44	-2.4%						-2.4%
Wagner, kω-Wilcox	6.78	2.7%					2.7%	
Wagner, Spalart-Allmaras	6.44	-2.4%			-2.4%			
Zeiss, SST	5.86	-11.2%	-11.2%					

Table 2: Comparison of axial Mach disc position

	Shock	Offset	SST	SST	Spalart	Baldwin	kω	kω	Offset
	X_{sh}/R^*	X_{shCFD}/X_{shexp}		modified	**Allmaras**	**Lomax**	Wilcox	Sarkar	X_{shCFD}/L
Experiment	9.85								9.4%
Alziary, SST stand., Gr.A	9.16	-7.0%	-7.0%						1.8%
Alziary, SST stand., Gr.B	9.18	-6.8%	-6.8%						2.0%
Alziary, SST stand., Gr.C	9.11	-7.5%	-7.5%						1.2%
Alziary, SST & Moore, Gr.B	8.90	-9.6%		-9.6%					-1.1%
Alziary, SST & Durbin, Gr.B	8.08	-18.0%		-18.0%					-10.2%
Alziary, SST & Pope, Gr.B	9.18	-6.8%		-6.8%					2.0%
Negishi, Baldwin-Lomax	8.53	-13.4%				-13.4%			-5.2%
Negishi, Spalart-Allmaras	9.48	-3.8%			-3.8%				5.3%
Negishi, SST mod.	8.91	-9.5%		-9.5%					-1.0%
Nasuti, Spalart-Allmaras mod.	8.92	-9.4%			-9.4%				-0.9%
Nasuti, Spalart-Allmaras	9.86	0.1%			0.1%				9.6%
Nebbache, SST	8.99	-8.7%	-8.7%						-0.1%
Östlund, SST/As=2.0	9.58	-2.7%		-2.7%					6.4%
Östlund, SST/As=3.23	9.14	-7.2%	-7.2%						1.6%
Östlund, SST/As=3.23, fine	9.14	-7.2%	-7.2%						1.6%
Ruf, kω-Sarkar	9.61	-2.4%						-2.4%	6.8%
Wagner, kω-Wilcox	9.54	-3.1%					-3.1%		6.0%
Wagner, Spalart-Allmaras	9.33	-5.3%			-5.3%				3.7%
Zeiss, SST	9.08	-7.8%	-7.8%						0.9%

Table 3: Nozzle contour and test case data

X/R*	R/R*	X/R*	R/R*	X/R*	R/R*	X/R*	R/R*	Reflected Shock	
-4.500	2.000	1.050	1.390	4.003	2.525	8.903	3.726	X/R*	Y/R*
-4.000	2.000	1.099	1.411	4.099	2.556	8.999	3.744	9.9714	2.2327
-3.000	2.000	1.148	1.433	4.203	2.588	9.000	3.744	10.1197	2.293
-2.600	2.000	1.199	1.455	4.301	2.619			10.2581	2.3532
-2.590	2.000	1.250	1.478	4.401	2.650	X/R*	P_{wall}/P_0	10.4164	2.3937
-2.588	2.000	1.302	1.500	4.501	2.680	0	0.378	10.5648	2.4341
-2.580	2.000	1.351	1.522	4.603	2.711	0.285	0.1395	10.733	2.4647
-2.550	1.999	1.400	1.543	4.609	2.713	0.47	0.1275		
-2.500	1.996	1.450	1.565	4.699	2.739	0.93	0.0869	Slip Line	
-2.450	1.990	1.501	1.587	4.802	2.770	1.39	0.0658	X/R*	Y/R*
-2.400	1.982	1.548	1.607	4.900	2.798	1.65	0.0564	9.9714	2.2327
-2.350	1.971	1.600	1.629	4.999	2.826	1.87	0.0512	10.1197	2.293
-2.300	1.958	1.649	1.650	5.099	2.855	2.07	0.045	10.2581	2.3532
-2.250	1.941	1.702	1.672	5.200	2.883	2.34	0.041	10.4164	2.3937
-2.200	1.922	1.751	1.693	5.301	2.911	2.81	0.0345	10.5648	2.4341
-2.165	1.906	1.801	1.714	5.403	2.939	3.26	0.028	10.733	2.4647
-2.160	1.904	1.852	1.735	5.500	2.965	3.75	0.024		
-2.150	1.899	1.899	1.755	5.597	2.991	4.24	0.0202	Mach Disc	
-1.250	1.480	1.950	1.776	5.701	3.018	4.72	0.0173	X/R*	Y/R*
-0.440	1.102	2.002	1.797	5.800	3.044	5.2	0.0153	9.8596	0.2242
-0.430	1.097	2.050	1.817	4.900	2.798	5.68	0.0137	9.8786	0.4529
-0.400	1.083	2.099	1.837	5.900	3.070	6.17	0.0122	9.8779	0.6617
-0.350	1.063	2.152	1.858	6.000	3.095	6.41	0.0118	9.8772	0.8505
-0.300	1.046	2.201	1.878	6.101	3.121	6.65	0.0165	9.8962	1.0792
-0.250	1.032	2.251	1.898	6.202	3.146	6.9	0.028	9.9252	1.2881
-0.200	1.020	2.301	1.918	6.298	3.169	7.1	0.0316	9.9343	1.5168
-0.150	1.011	2.352	1.938	6.401	3.195	7.4	0.0338	9.9336	1.7355
-0.100	1.005	2.398	1.956	6.498	3.218	7.63	0.0352	9.9427	1.9542
-0.050	1.001	2.450	1.976	6.602	3.243	7.89	0.0358	9.9421	2.1132
0.000	1.000	2.501	1.996	6.700	3.266	8.12	0.0364	9.9714	2.2327
0.050	1.002	2.549	2.014	6.799	3.289	8.36	0.0369		
0.101	1.010	2.601	2.034	6.898	3.312	8.62	0.0373		
0.150	1.023	2.649	2.053	6.998	3.335				
0.200	1.040	2.698	2.071	7.099	3.358	Oblique Shock			
0.250	1.057	2.751	2.091	7.200	3.380	X/R*	Y/R*		
0.300	1.075	2.801	2.109	7.302	3.403	9.1086	2.6562		
0.350	1.094	2.850	2.128	7.397	3.423	9.2077	2.6069		
0.399	1.113	2.900	2.146	7.500	3.446	9.3367	2.5479		
0.450	1.133	2.950	2.164	7.604	3.468	9.4556	2.4987		
0.501	1.154	3.000	2.183	7.700	3.488	9.5945	2.4297		
0.552	1.175	3.005	2.185	7.798	3.509	9.7036	2.3706		
0.599	1.194	3.097	2.218	7.903	3.531	9.8227	2.2916		
0.650	1.216	3.200	2.254	8.001	3.551	9.9714	2.2327		
0.700	1.237	3.299	2.289	8.100	3.571				
0.749	1.258	3.399	2.324	8.200	3.591				
0.802	1.281	3.501	2.359	8.300	3.611				
0.849	1.302	3.598	2.392	8.400	3.631				
0.898	1.323	3.702	2.427	8.502	3.650				
0.951	1.346	3.801	2.459	8.603	3.670				
1.002	1.369	3.901	2.492	8.697	3.688				

This page has been purposedly left blank